Materials Today Sustainability 30 (2025) 101087

Contents lists available at ScienceDirect

Materials Today Sustainability

journal homepage: www.journals.elsevier.com/materials-today-sustainability

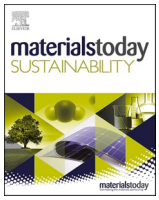

Optimising slow pyrolysis parameters to enhance biochar European hazelnut shell as a biobased asphalt modifier

Camila Martínez-Toledo [a,b], Gonzalo Valdes-Vidal [b,*], Alejandra Calabi-Floody [b], María Eugenia González [c], Antonieta Ruiz [c], Cristian Mignolet-Garrido [b], Jose Norambuena-Contreras [d]

[a] Engineering Doctoral Program, University of La Frontera, Temuco, 4811230, Chile
[b] Department of Civil Engineering, University of La Frontera, Temuco, 4811230, Chile
[c] Department of Chemical Engineering, University of La Frontera, Temuco, 4811230, Chile
[d] Materials and Manufacturing Research Institute, Department of Civil Engineering, Faculty of Science and Engineering, Swansea University, Bay Campus, SA1 8EN, UK

ARTICLE INFO

Keywords:
Pyrolysis
Biochar
European hazelnut shell
Asphalt binder

ABSTRACT

This paper evaluated the impact of operational conditions during slow pyrolysis on the physicochemical and antioxidant properties of biochar derived from European hazelnut shells (BH), with the aim of assessing its potential as a modifier for asphalt binder. The study employed a 2^2 factorial design with a central point, using pyrolysis temperature (300 °C, 425 °C, and 550 °C) and residence time (1, 2, and 3 h) as study factors to produce BH. Firstly, the chemical, physical and antioxidant properties of European hazelnut shell (HS) and BH samples were compared in terms of their chemical composition, microscopic-morphology, and antioxidant capacity. Additionally, the thermal behaviour of HS was analysed. Asphalt binders were blended with 5% biochar (w/w) to assess particle distribution using confocal laser microscopy. Functional groups were also evaluated through Fourier-transform infrared spectroscopy (FT-IR) and X-ray photoelectron spectroscopy (XPS). The results conclude that the operational conditions of slow pyrolysis significantly affect the chemical composition of biochar from European hazelnut shells, influencing the functional groups present on the asphalt surface. These conditions also influence the microstructure, increasing porosity and rugosity at higher temperatures and longer residence times. HS exhibited high antioxidant capacity, retaining up to 40% of it in the biochar when pyrolyzed at 300 °C for 1 h. Confocal laser microscopy showed uniform distribution of biochar in the asphalt binder. FT-IR and XPS tests revealed chemical interactions between the biochar and binder, characterized by bonds involving C, O, and H, particularly in biochar pyrolyzed at 300 °C and 550 °C for 1 h. The results of this study demonstrate that biochar derived from the slow pyrolysis of European hazelnut shell has the potential to be used as a bio-additive for the development of more sustainable asphalt roads.

1. Introduction

During the last decades, asphalt pavements have deteriorated significantly, largely due to a substantial increase in heavy vehicle traffic and challenging environmental conditions, particularly the rising temperatures linked to climate change [1,2]. This has affected the asphalt paving industry, as asphalt pavements are the most commonly used material for road and highway construction. In fact, 86% of the paved road network in Chile and over 95% globally consist of asphalt pavement [3–5]. In this regard, modifying asphalt binder to improve its properties has become a key area of research and development, as it is a crucial organic compound for the mechanical performance of pavements [6]. In addition to the growing emphasis on the circular economy, the development of alternative bio-additives derived from waste produced by various agroindustries has recently gained significant attention. In this context, the European hazelnut (*Corylus avellana* L.) agroindustry has seen a notable increase [7]. According to the latest statistics from the Food and Agriculture Organization (FAO), in 2022, approximately 1 million tons of hazelnuts (including shells) were produced, marking a 50% increase over the past decade [8]. Nearly 90% of the world's hazelnut production is concentrated in Asia and Europe, with Turkey leading the way at 765,000 tons, which accounts for more than 70% of

* Corresponding author.
E-mail address: gonzalo.valdes@ufrontera.cl (G. Valdes-Vidal).

https://doi.org/10.1016/j.mtsust.2025.101087
Received 27 August 2024; Received in revised form 13 January 2025; Accepted 8 February 2025
Available online 13 February 2025

global production and 82% of exports [7,8]. Latin America contributes approximately 10% to the global hazelnut production, with Chile being the leading producer in the region at 62,557 tons. This positions Chile as the fifth-largest hazelnut producer in the world [8]. These values indicate ongoing growth in both hazelnut production and the cultivated area, suggesting an increase in the volume of by-products generated from processing. This, in turn, presents a challenge in managing the solid waste materials generated by the industry [9]. One of these challenges involves managing hazelnut shells, which constitute between 50% and 70% of the total weight of a hazelnut, depending on the variety and cultivation practices [9,10]. This translates to over 830,000 tons of hazelnut shells (HS) generated worldwide from processing in 2022.

Various treatments are currently under investigation for recycling HS, including their use as adsorbents for environmental contaminants such as CO_2 [11]. They have also been used for ethanol production [12], as well as to extract phenolic compounds [7,13]. These compounds are characterised by their high antioxidant capacity and various potential uses in bioactivity [7]. Studies have demonstrated that hazelnut by-products, such as the shells, contain a higher concentration of phenolic compounds compared to the hazelnut itself [13]. The identified phenolic compounds encompass phenolic acids, flavonoids, tannins, diarylheptanoids, and lignins, all of which are known for their potent antioxidant properties [7,10,14]. Likewise, the HS contain large quantities of lignin (40–50% w/w), hemicellulose (13–32% w/w) and cellulose (16–27% w/w) [7,9,15], making them a valuable source of natural antioxidant compounds.

One approach to recycle hazelnut shells through bio-refining involves thermochemical conversion via pyrolysis [16]. Pyrolysis is a thermochemical process that converts biomass into biochar, bio-oils, and biogas in an oxygen-free environment, typically at temperatures ranging from 300 to 1000 °C [16,17]. The solid product obtained from pyrolysis, known as biochar, is a carbon-rich material with high calorific value and a large, porous surface area [17]. The elemental composition and physical-chemical properties of biochar largely depend on the biomass composition and the conditions of pyrolysis, including temperature, residence times, and heating rate [17]. Studies have demonstrated that at lower temperatures, between 350 and 650 °C, the chemical bonds in biomass undergo rupture and reorganization, resulting in the formation of new functional groups such as carboxyl, lactone, lactol, quinone, chromene, anhydride, phenol, ether, pyrone, pyridine, pyridone, and pyrrole [18]. In contrast, at higher temperatures (above 650 °C), the Cation Exchange Capacity (CEC) and the content of surface functional groups containing hydrogen and oxygen decrease [18]. Furthermore, higher levels of lignin in the biomass lead to increased production of phenolic compounds in the resulting biochar [19]. Along with the selection of feedstock, pyrolysis operating conditions such as heating rate, residence time, and temperature can significantly affect the cost of biochar production, primarily due to energy consumption [20,21]. In this regard, the operating conditions of pyrolysis determine whether it is classified as slow or fast pyrolysis [20]. Slow pyrolysis is typically conducted at temperatures between 350 °C and 800 °C and involves a longer residence time, often lasting several minutes or even hours [22]. It also produces a higher biochar yield (approximately 30%), with costs ranging from 35 to 40 USD per tonne of biochar, excluding transport costs [23]. Fast pyrolysis, on the other hand, is carried out at temperatures between 425 °C and 550 °C with a much shorter residence time, typically ranging from 1 to 2 s. It also results in a lower biochar yield (around 12%) and is therefore commonly used for bio-oil production [23,24].

The use of pyrolyzed biochar to modify asphalt binder enables the conversion of waste into value-added products, thereby promoting the circular economy in other industries. Consequently, this technology contributes to sustainable development, addressing both industrial needs and the demands of contemporary society [21,25,26]. In this context, various studies have been conducted on the modification of asphalt binder with biochar. Martínez-Toledo et al. found that there is a strong physicochemical interaction between oat hull biochar, produced through slow pyrolysis at 300 °C with a 2-h residence time, and asphalt binder [27]. This interaction is attributed to the porous morphology of the biochar and the C═O and C═C bonds in the functional groups present in both materials, which allow the viscoelastic working range of the biochar-modified asphalt binder to be extended. Furthermore, the modified asphalt binders exhibited good storage stability.

Similarly, Zhou et al. [28] found that biochar derived from cypress wood waste contributes aromatic and aliphatic compounds to the asphalt, while also promoting the production of aromatics. This leads to enhanced resistance to both oxidation and ageing. On the other hand, Zhang et al. studied the effect of different particle sizes of biochar derived from wood residues, obtained from pyrolysis treatment carried out between 500 and 650 °C with a heating rate of 104–105 °C/min, on the rheological properties of asphalt binder [29]. The results indicated that the biochar exhibits a porous and rough surface texture, which enhances the adhesion interaction with the asphalt binder. This increases its rotational viscosity, as well as its resistance to rutting and ageing, particularly when biochar with a particle size of less than 75 μm is applied. Additionally, improved crack resistance at low temperatures was observed. In the same context, Gan and Zhang [30] analysed the effect of biochar generated from the pyrolysis of straw in a muffle furnace at 450 °C for 1 h residence time, obtaining similar results regarding the increase of the rotational viscosity in biochar-modified asphalt binders. Similarly, for Ma et al. [31] investigated the effect of biochar DS-510F as an asphalt binder modifier, finding that it was composed of aromatic rings, alkanes, and hydroxyl groups, which enhanced the viscosity and properties of the asphalt binder at high temperatures. On the other hand, Hua et al. [32], by using a biochar from the pyrolysis of straw stalks composed of a relative content of aromatic C–O bonds, aromatic carbons and alkyne carbons, obtained similar results. Finally, Walters et al. [33] found that the amount of biochar derived from the residue of a thermochemical process that converts pig manure into bio-oil is directly proportional to the increase in the viscosity of the modified asphalt binder. Additionally, this biochar was found to reduce the thermal susceptibility of the binder.

Based on the previous discussion, the scientific novelty of this study lies in the exploration of influential variables that can enhance the effect of biochar on the modification of asphalt binders. These include the use of an antioxidant-rich biomass source such as HS, biochar particle sizes within the range suitable for coating the asphalt binder on aggregates (e.g., under 20 μm), and variations in low pyrolysis operational conditions to improve the physicochemical interaction between the asphalt binder and the biochar. To the best of our knowledge, these factors have not yet been studied. For this reason, this study aimed to assess how the operational conditions of slow pyrolysis affect the physical-chemical and antioxidant properties of European hazelnut shell biochar (BH), with the potential application as a modifier for asphalt binder. Besides, considering the growing demand for European hazelnuts, exploring this biochar as a potential bioadditive for the road-surfacing industry is of particular interest, as it could enhance the mechanical performance of asphalt paving.

2. Materials and methods

2.1. Materials

The biochar used in this study was produced from European hazelnut shells, HS (*Corylus avellana* L.) obtained from the Araucanía Region of Chile. It was produced through slow pyrolysis under various operational conditions of temperature and residence time. Pyrolysis was carried out in a stainless steel fixed-bed chamber with approximate volume 0.117 m^3. The temperature was increased at a constant rate of 3.6 °C/min, controlled by a Thermocouple Type K sensor (NiCr–Ni) connected to a PID regulator. Inert gas (N_2) was introduced at a constant flow of 0.001 m^3/min to purge the oxygen generated during pyrolysis. The liquid

fraction generated by pyrolysis was separated using a volatiles condenser, which allowed the bio-oil to be collected in a TAR container, while the biogas was released into the environment. The biochar collected in the chamber was allowed to cool to ambient temperature and then subjected to size reduction to obtain particles smaller than 20 μm. Fig. 1 illustrates the experimental four-stages through which the biochar was obtained to be characterised. Additionally, Table 1 displays the properties of the asphalt binder used in this study, classified under Chilean regulations as type PG 64-22.

2.2. Experimental design

The study comprised three stages to achieve the intended objective. Firstly, a physical-chemical characterisation of the European hazelnut shells (HS) was conducted before pyrolysis. In the second stage, a 2^2 factorial design with a central point was implemented using Design Expert software (refer to Table 2) to investigate the effects of pyrolysis temperature (300 °C, 425 °C, and 550 °C) and residence time (1, 2, and 3 h) on the properties of the biochar, aimed at assessing its potential use as an asphalt binder modifier. Finally, in the third stage, the physical-chemical interaction of the biochar with the asphalt binder after modification was evaluated.

2.3. Modification of the asphalt binder with the biochar

Fig. 2 shows the experimental design for modification of the asphalt binder with biochar; the mixing conditions were chosen based on the results obtained by Martínez-Toledo et al. [27]. First, the asphalt binder was pre-heated in an oven to 130 ± 5 °C for 30 min to make it more workable. Next, 650 g of asphalt binder were heated on a heating plate to the mixing temperature of 160 ± 5 °C. Then 5% of biochar (w/w of the asphalt binder) was added gradually, keeping a constant stirring velocity of 350 rpm for 30 min. At the end of this time, the modified asphalt binder was kept at 120 °C for a further 6 h to improve adsorption of the asphalt on the biochar particles [30]. The analysis matrix included seven samples: "AB" (asphalt binder without modification procedure or biochar), "AB+0" (asphalt binder with modification procedure but without biochar) and "AB + X" (where "X" represents BH1, BH2, BH3, BH4 and BH5). Except for AB, all the test samples were prepared using the same modification procedure.

2.4. Test methods

2.4.1. Chemical characterisation

At macromolecular level, the chemical composition of the HS and the biochar was determined by the organic elemental analysis method (CHNS), using an EA-3000 elemental analyser (EuroVector, Pavia, Italy). This gave the C, H, N and S contents, while the O content was calculated by equation (1):

$$O = 100 - C - H - N \quad (1)$$

Table 1
Properties of the asphalt binder PG 64-22 used in the study.

Test Parameter	PG 64-22	Specification
Properties of original binder		
Rotational Viscometer at 135 °C, (Pa·s)	0.313	3.000 Max.
Dynamic Shear, G*/sinδ at 64 °C, (kPa)	1.150	1.000 Min.
Properties of binder from rolling thin film oven (RTFO)		
Mass Loss, (%) weight	−0.101	1.000 Max.
Dynamic Shear, G*/sinδ at 64 °C, (kPa)	2.380	2.200 Min.
High critical temperature, (°C)	64.703	64.000 Min.
Properties of binder from pressure aging vessel (PAV)		
Dynamic Shear, G*sinδ at 25 °C, (kPa)	3616.654	5000.000 Max.
Intermediate critical temperature, (°C)	22.600	25.000 Max.
Creep stiffnes, S-value at −12 °C, (MPa)	230.121	300.000 Max.
Creep stiffnes, m-value at −12 °C	0.316	0.300 Min.
Low critical temperature, (°C)	−23.602	−22.000 Max.

Table 2
Factorial design 2^2 with a central point.

Sample	Temperature (°C)	Time of residence (h)
BH1	300	1
BH2	300	3
BH3	425	2
BH4	550	1
BH5	550	3

where O is the oxygen concentration in (%), C is the carbon concentration in (%), H is the hydrogen concentration in (%) and N is the nitrogen concentration in (%).

To determine the chemical composition at the micromolecular level, the Total Reflection X-ray Fluorescence (TXRF) method was employed using an S2 PUMA instrument (Bruker, Billerica, MA, USA) with excitation set at 50 kV and 2 mA. The functional groups on the surface of the HS and of the biochar samples were identified by Fourier-transform infrared spectroscopy (FT-IR), using a Cary 630 FTIR spectrometer (Agilent Technologies, Santa Clara, CA, USA) with diamond attenuated total reflectance (ATR). The IR spectra were between 4000 cm^{-1} and 600 cm^{-1}. Finally, the total, carboxylic and phenolic acidity of the biochar samples were measured by potentiometric titration. In the case of the total acidity, the barium hydroxide $Ba(OH)_2$ method was used [34]. For the carboxylic acidity, the calcium acetate $Ca(CH_3COO)_2$ method was used. The phenolic acidity was calculated from the difference between the total acidity and carboxylic acidity.

2.4.2. Physical characterisation

The microscopic morphologies of the HS and the biochar samples were obtained by Scanning Electron Microscopy (SEM), using an EVO I MA10 microscope (Carl Zeiss, Jena, Germany) in operating conditions of 20 kV with the primary electron detector. In this case, the samples were first coated with approximately 60 nm of gold, using the Q150R ES plus metallizer (Quorum Technologies, Lewes, United Kingdom). The

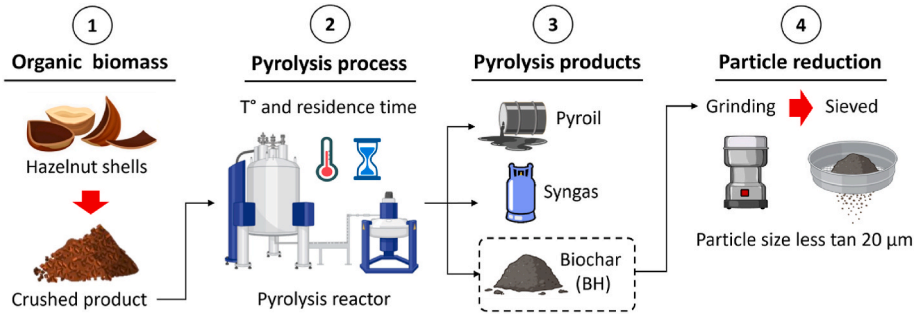

Fig. 1. Diagram illustrating the experimental process for obtaining the biochar used in the study.

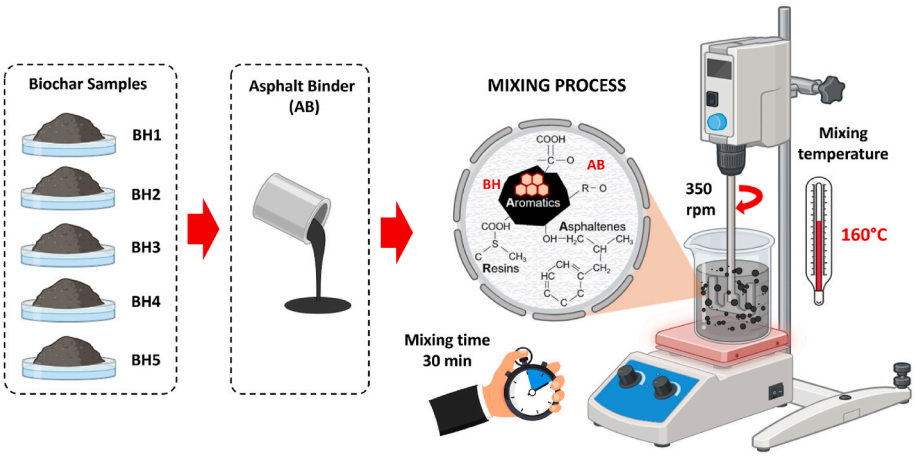

Fig. 2. Diagram of the experimental process for asphalt binder modification with biochar.

specific surface area (S_{BET}), pore volume (Vp) and pore diameter (Dp) of the biochar samples were determined using a NOVA 1000e porosimeter (Quantachrome Instruments, Boynton Beach, FL, USA), by adsorption and desorption of nitrogen at 77 K on samples previously dried and degasified at 160 °C for 16 h. The S_{BET} was measured using the method of Brunauer-Emmett-Teller, and the Vp with the Barrett-Joyner-Halenda method. The particle size of the biochar was measured by laser diffraction using the SALD-3101 DRY equipment (Shimadzu, Kioto, Japan), with a refraction index of 2.00–0.20i. The surface charge of the biochar was determined by the Z-potential using a Zetasizer Nano ZS (Malvern Instruments, United Kingdom). The Z-potential was measured by fitting to the Smoluchowski model with f (ka) measurement of 1.5, based on the electrophoretic mobility measured with a DTS1070C cell (Malvern Instruments, United Kingdom). Finally, the production yield of the biochar was calculated by equation (2):

$$R = (m_f / m_i) \bullet 100\% \quad (2)$$

where R is the production yield of biochar in (%), m_f is the mass of the biochar after pyrolysis in (g) and m_i is the mass of the HS before pyrolysis in (g); in this case m_i was equal to 1000 g.

2.4.3. Characterisation of antioxidant properties

The antioxidant activity of the HS and the biochar samples was evaluated by the oxygen radical absorption capacity (ORAC), the Trolox equivalent antioxidant capacity (TEAC), the 2,2-diphenyl-1-picrylhydrazyl (DPPH) and the cupric reducing antioxidant capacity (CUPRAC) methods, as follow.

1 *ORAC method*: was determined using the methodology described by Cao et al. [35], measuring the fluorescence of the solution containing the sample every 5 min for a total of 90 min. A Synergy HTX multimode reader (BioTek, Winooski, VT, USA) was used, and the values were expressed in Trolox equivalent μmol g^{-1}.
2 *TEAC method*: the solutions were adjusted to an absorbance of 0.70 ± 0.05 (734 nm) by dilution with ethanol or water before use [36]. In a 96-well plate, 245 μL of $ABTS^{+\cdot}$ 7.5 mM, previously diluted, was added (A1) together with 5 μL of Trolox standard or sample and then incubated for 30 min at 30 ∘C (A2). The measurements were taken with a UV–Vis Epoch Microplate Spectrophotometer (BioTek, Winooski, VT, USA), and the values were expressed in Trolox equivalent μmol g^{-1} [37].
3 *DPPH method*: was determined using the methodology described by Maldonado et al. [38], with some modifications. The first absorbance reading was carried out in a 96-well plate with 240 μL of 0.1 mM DPPH dissolved in ethanol. For the second reading, 10 μL of the Trolox curve or the sample were added, and the solution was incubated for 30 min in darkness. The measurements were taken at 517 nm with a UV–Vis Epoch Microplate Spectrophotometer (BioTek, Winooski, VT, USA), and the values were expressed in Trolox equivalent μmol g^{-1}.
4 *CUPRAC method*: was determined based on the methodology described by Joana et al. [39]. Briefly, in a 96-well plate, 50 μL of 10 mM $CuCl_2$, 50 μL of 7.5 mM neocuproine and 50 μL of 1 M ammonium acetate buffer pH 7 was added and incubated at 27 °C for 15 min. Then,100 μL of Trolox standard, or sample, was added and incubated for30 min at 27 °C. The absorbance was determined at 450 nm using a UV–Vis Epoch Microplate Spectrophotometer (BioTek, Winooski, VT, USA), and the values were expressed in Trolox equivalent μmol g^{-1}.

Additionally, the Total Polyphenols Content (TPC) was determined using the Folin-Ciocalteu method as described by Singleton et al. [40]. The absorbance was measured at 750 nm with a UV–Vis Epoch Microplate Spectrophotometer (BioTek, Winooski, VT, USA). The determinations were performed using gallic acid as the standard; the concentrations in the calibration curve corresponded to 100, 200, 300, 400 and 500 mg L^{-1}.

2.4.4. Thermal behaviour

The thermal behaviour of the HS was determined by thermogravimetric analysis (TGA), using a STA 6000 (PerkinElmer, Shelton, CT, USA). The initial condition used was with 20 mg of sample with a flow of N_2 of 40 ml/min; the temperature was increased from 25 °C to 900 °C at a heating rate of 20 °C/min.

2.4.5. Interaction between the asphalt binder and biochar

The distribution and integration of the biochar in the asphalt binder were determined using confocal laser microscopy, using a FV1000 equipment (Olympus, Tokyo, Japan). Subsequently, the interaction between the asphalt binder and each biochar was evaluated using FT-IR, identifying the emergence of new functional groups or the modification of existing ones in their respective IR spectra. This evaluation was carried out after the modification procedure, using a Cary 630 FTIR spectrometer (Agilent Technologies, Santa Clara, CA, USA) with ATR between 4000 cm^{-1} and 600 cm^{-1}. Finally, the functional groups were quantified after the modification procedure by X-ray photoelectron spectrometry (XPS), using a Surface Analysis Station 2 XPS RQ300/2 (Staib Instrument GmbH, Langenbach, Germany). The spectra were obtained with Al radiation (1486.6 eV) and a calibration value C of 284.8 eV.

3. Results and discussion

3.1. Characterisation of the European hazelnut shells and biochar

3.1.1. Chemical properties

Table 3 compares the chemical composition of the biochar samples at macro- and micromolecular levels, with reference to the composition of the HS. At macromolecular level, the most abundant chemical elements in the HS were C and O, together totalling more than 91% of the total composition. H and N were detected in smaller concentrations, H being the third most abundant element. S was imperceptible by the analytical method used, suggesting that it might be present in a concentration below the limit of detection. According to the literature, HS is composed principally of C (46–51%), followed by O (42–48%), H (5–6%), N (0.1–0.4%) and S (0.05–0.7%). Thus, the results obtained were similar to those reported in other studies [30–35]. Furthermore, at micromolecular level, Ca and K are the most abundant chemical elements (0.39 and 0.32%, respectively). These are two of the essential nutrients for establishing a hazelnut orchard [41]. Other elements detected included Si, Fe, and S, in concentrations lower than 0.07%. This could be attributed to the growing conditions of the trees, as well as interactions with soil and climate factors unique to each region where they are cultivated [41,42].

At the macromolecular level, it can be observed that pyrolysis at higher temperatures and with longer residence times significantly increases the carbon (C) content in the biochar (see Table 3). This may be advantageous for modifying asphalt binder (P-value = 0.000 of the ANOVA), the carbon content being approximately 35–83% higher than in HS. According to the literature, this phenomenon may be attributed to a series of reactions occurring during pyrolysis, including dehydration, condensation, polymerisation and aromatisation [43,44]. On the other hand, the oxygen (O) and hydrogen (H) contents decreased significantly compared to the content in HS. (P-value = 0.000 in the ANOVA). This is because as the pyrolysis temperature increases, more elemental oxygen and hydrogen are released in the gaseous and condensable phases [45,46]. For this reason, biochar pyrolyzed at 550 °C, both for 1 h and for 3 h, presented lower values for these elements, with O varying between 35 and 85% and H between 32 and 64%. The N and S contents are low (less than ~1%), which is advantageous, since a high content of these elements may cause NO_x and SO_x emissions, depending on use [47]. On this context, Zhao et al. [48] reported similar values for biochar from hazelnut shells, indicating that after pyrolysis at temperatures between 400 and 600 °C, and residence time of 20 min, they measured ~55–71% of C, ~25–40% of O, ~2–3% of H and ~0.05–0.10% of N.

Table 3
Chemical composition of biochar at macro- and micromolecular levels, with reference to HS.

Chemical element	HS	BH1	BH2	BH3	BH4	BH5
	Mean (%)					
Macromolecular level						
N	0.585	0.591	0.584	0.934	0.926	0.536
C	49.365	66.627	68.932	74.720	84.576	90.366
O	42.143	27.373	25.248	20.418	11.542	6.219
H	7.907	5.410	5.236	3.928	2.956	2.879
S	ND	ND	ND	ND	ND	ND
Micromolecular level						
Cr	–	0.014	0.040	0.015	0.054	0.072
Mn	0.004	0.009	0.010	0.009	0.009	0.016
Fe	0.030	0.160	0.260	0.150	0.390	0.500
S	0.020	0.018	0.020	0.019	0.026	0.032
P	0.004	–	–	–	–	0.006
Si	0.070	–	–	–	–	–
Mg	–	0.100	–	–	–	–
K	0.320	0.620	0.510	0.770	0.810	0.800
Ca	0.390	0.730	0.590	0.910	0.650	0.820
Sc	0.002	0.007	0.006	0.009	0.008	0.006
Ti	–	0.019	0.012	–	–	0.014
Ni	–	–	0.025	–	0.023	0.022
Cu	–	–	–	–	–	0.020
Zn	–	0.024	0.019	0.019	0.020	0.025
Ag	0.003	0.004	0.004	0.004	0.004	0.004
Rh	–	–	0.005	0.005	–	–
Pd	0.016	0.012	0.014	0.012	0.013	0.011
Sr	–	0.018	0.017	0.019	0.019	0.021
Rb	–	0.017	0.017	0.018	0.020	0.020
Cl	0.002	0.009	0.009	0.022	0.020	0.058
Eu	0.014	0.038	0.033	0.041	0.035	0.036
Tb	–	0.024	0.026	0.022	0.033	0.029
Dy	–	–	–	–	–	0.015

Note: ND: Not Detected, outside detection limit (1.200%).

At micromolecular level (see Table 3), it was observed that the biochar are rich in chemical elements, with Ca, K and Fe the most abundant, similar to the composition of HS. However, the increase in these concentrations does not exhibit a clear pattern related to the pyrolysis conditions evaluated.

Fig. 3 shows the IR spectra of HS and biochar samples, indicating the bands where functional groups characteristic of their surfaces are located. According to the HS spectrum, a peak is observed at 3355 cm^{-1} which corresponds to the –OH hydroxyl group. This is attributable to the stretching vibrations caused by hydrogen bonds at the inter- and intramolecular levels in polymer compounds such as lignin and cellulose, which are typical of HS [49]. At 2925 cm^{-1} and 2848 cm^{-1} peaks were found corresponding to the strong symmetrical stretching of the C–H bonds of the $–CH_3$ and $–CH_2$ functional groups respectively. A 2320 cm^{-1}, 2100 cm^{-1} and 1990 cm^{-1} stretching attributed to the –C ≡C– alkyne bonds was recorded, while at 1733 cm^{-1} was the peak corresponding to stretching of the –C═O carbonyl group, present in carbohydrates and lignin [50,51,52]. At 1597 cm^{-1} and 1508 cm^{-1} the bond vibrations of aromatic rings were found [49,51,52,53], while between 1454 cm^{-1} and 1317 cm^{-1} we recorded the peaks corresponding to the flexion vibrations of the –OH bonds and the deformation vibrations of the methyl and methylene functional groups of lignin and cellulose [51]. Finally, at 1225 cm^{-1} the –C–O– bond vibrations appear, attributable to alcohols, aliphatic ethers, phenols and carboxylics, and at 1025 cm^{-1} the strong stretching corresponding to the –COC– group can be identified, caused by the flexion vibrations of the hemicellulose and cellulose of the HS, as reported in Refs. [51,52].

According to the spectra of the biochar samples (see Fig. 3), first it can be seen that the peak at 3349 cm^{-1}, which corresponds to the hydroxyl –OH group, tends to disappear in the biochar pyrolyzed at temperatures above 300 °C. This may be due to the diminution of lignocellulose O and H in the gaseous and vapour phases of pyrolysis [45,46]. This means that only the biochar generated at 300 °C for 1 and

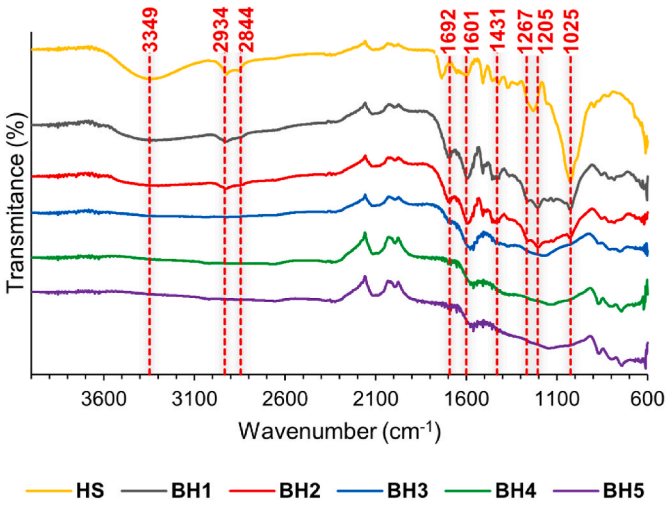

Fig. 3. IR spectra with functional groups characteristic of the HS and the biochar samples.

3 h would conserve part of the antioxidant capacity of HS associated with this hydroxyl group [54–56]. At 2934 cm^{-1} and 2844 cm^{-1}, the C–H bonds of the $–CH_3$ and $–CH_2$ functional groups respectively also tend to disappear due to the effect of the temperature on H elements. At 1692 cm^{-1}, the peak corresponding to the stretching of the –C═O carbonyl group, present in carbohydrates and lignin, also tends to diminish because of temperature on O [50,51,52]. At 1601 cm^{-1} the bond vibrations of aromatic rings are conserved, but at a pyrolysis temperature of 550 °C they tend to shift to a lower energy value [49,51, 52,53]. At 1431 cm^{-1} the biochar present an increase in the peaks corresponding to the deformation vibrations of the methyl and methylene functional groups of the HS lignin and cellulose [51]. Finally, the peaks corresponding to the –C–O– bond vibrations and the strong stretching of the –COC– group of the HS tend to be reordered and disappear in the biochar pyrolyzed at over 300 °C. They are therefore only observed in the form of small signals at around 1267 cm^{-1}, 1205 cm^{-1} and 1025 cm^{-1}.

Table 4 shows the values obtained for the acidity of the biochar samples, comparing them with those of HS. Based on this, the factorial model indicated that both the pyrolysis temperature and residence time, as well as curvature, do not have a significant effect on the total acidity of the biochar (P-values = 0.150, 0.500, and 0.872, respectively). However, upon separate analysis, it is observed that the total acidity and phenolic acidity vary more between samples than carboxylic acidity does, indicating a greater influence of the pyrolysis parameters on these aspects. From this, it appears that biochar pyrolyzed at 300 °C for 1 and 3 h has greater phenolic acidity due to the presence of –OH hydroxyl functional groups (see Fig. 3). This evidence may be beneficial for the asphalt binder, as these phenolic compounds contribute antioxidant activity against photo-oxidation and oxidation [57]. These same biochar samples (pyrolyzed at 300 °C for 1 and 3 h) presented the highest values for carboxylic acidity. This may be because of the carboxylic groups present in these biochar samples, which are connected to the following bonds: carbon-oxygen double bond (C═O), simple carbon-oxygen stretching bond (C–O) and oxygen-hydrogen bond (O–H), which are related with the resistance to fatigue and rutting of the asphalt binder [58]. In the findings reported by González et al. [59], a similar composition is observed in the distribution of acidity in biochar produced from oat hulls and pine bark, with higher levels of phenolic than carboxylic acidity.

3.1.2. Physical properties

Fig. 4(a) shows the S_{BET} of the biochar samples analysed. It can be seen that increases in pyrolysis temperature and residence time lead to an increase in the S_{BET} of the biochar. This may be due to the decomposition of the components of the HS, such as cellulose, hemicellulose and lignin, which decompose at the pyrolysis temperatures used (see Fig. 10) [47,60]. Furthermore, this could encourage the development of particles with increasingly irregular and porous shapes and surfaces [61–63]. It should be noted that a greater surface area and porous structure facilitate the adhesion of biochar to the asphalt binder, enabling better interaction between their components [64]. When the characteristics of the pores are analysed, Fig. 4(b) shows that, for the same pyrolysis temperature, the longer residence time (3 h) generates an increase in Dp and diminution in Vp. This means that the pores are broad, shallow cavities, with volumes of around 0.004–0.039 cc/g. The Dp can be classified as mesopores for all the biochar samples analysed, having pores with internal diameter of between 2 and 50 nm [65]. Fig. 4 (c) shows the distribution of biochar particle sizes. From these results it can be calculated that the quantity of particles smaller than 20 μm is 69.29%, 65.18%, 73.14%, 75.07% and 84.86% for BH1, BH2, BH3, BH4 and BH5, respectively. This indicates that, overall, the sizes achieved in the grinding process meet the requirements established for the investigation, as confirmed by the descriptive parameters of particle size distribution. Fig. 4(d) shows that the mean sample size is between 6.53 and 12.06 μm, with the smallest particles belonging to the biochar pyrolyzed at 550 °C for 3 h. This is attributed to the decomposition of lignin, which makes it the material most prone to disintegration during grinding [47, 60,66].

Fig. 5(a)–(d) shows the microscopic morphology of the HS at different magnifications. Despite originating from the same raw material, particles with heterogeneous geometries and surfaces can be observed. Firstly, the HS have some particles with very compact surfaces (see Fig. 5(a)), which are attributed to the high lignin content in this type of biomass (approx. 40–50% w/w [7,9,15]). This serves as an agglutinant between the hemicellulose and cellulose of the cells [66]. In addition, these particles present porous zones (Fig. 5(b)) but smaller than those of biochar [47]. The HS also contain particles with rough surfaces, which at greater amplification are seen to have a fibrous appearance (see Fig. 5(c) and (d)) [50].

Fig. 6(a)–(e) shows the microscopic morphology of the biochar samples. With higher pyrolysis temperature and residence time, the particles acquire more irregular shapes and surfaces. This is attributed to the decomposition of the lignocellulose components of HS [47,60,66]. Furthermore, its decomposition contributes to the formation of solid carbon and determines its microporosity [66,67]. When these findings are compared with the S_{BET} results shown in Fig. 4(a), it can be deduced that the increase of pores and rough zones could contribute to the increase in the specific surface area of the biochar, which is largest in the biochar pyrolyzed at 550 °C for 1 and 3 h. According to existing literature, these attributes may enhance the physical interaction with the asphalt binder, potentially improving its resistance to rutting and rotational viscosity, as observed with biochar from switchgrass, waste wood and straw [30,64,68].

Moreover, Fig. 7 shows the mean Z-potential (ZP) of the biochar samples analysed. The ZP is associated with the surface charge of particles, as it represents the potential difference between the biochar and the surrounding medium. It offers insights into their behaviour and stability in solution, influenced by the repulsion between particles [69, 70]. On the basis of these results, the factorial model indicated that both the pyrolysis temperature and the residence time, as well as interaction between them, present no significant effect on the ZP of the biochars (P-values = 0.910, 0.388 and 0.490 respectively). For this reason, the results obtained were similar, with negative ZP values ranging between −37.7 and −42.3 mV. This indicates optimum particle dispersion for the values obtained [71].

According to the literature, the ZP of biochar varies with its pH, typically showing increasingly negative values as the pH rises and surpasses the corresponding isoelectric points. This also suggests a negative surface charge [72,73]. In practice, the higher the pH of the biochar, the better the potential interaction with calcareous aggregates and asphalt, possibly due to the acidity of the latter. This interaction could help mitigate stripping issues in asphalt mixtures [74]. Below we show some examples of biochar from different raw materials which illustrate the relation between the pH and ZP mentioned above: rice straw (pH 8 and

Table 4
Measurement of total, phenolic and carboxylic acidity in biochar samples compared to HS.

Parameter (in $mEq{\cdot}mg^{-1}$)	Total acidity	Carboxylic acidity	Phenolic acidity
HS	3.394 ± 2.154	0.191 ± 0.082	3.203 ± 2.070
BH1	4.033 ± 0.346	0.462 ± 0.073	3.571 ± 0.421
BH2	3.956 ± 0.816	0.463 ± 0.028	3.493 ± 0.844
BH3	0.470 ± 0.001	0.319 ± 0.027	0.151 ± 0.002
BH4	1.244 ± 0.269	0.430 ± 0.048	0.814 ± 0.311
BH5	1.787 ± 0.132	0.255 ± 0.199	1.532 ± 0.332

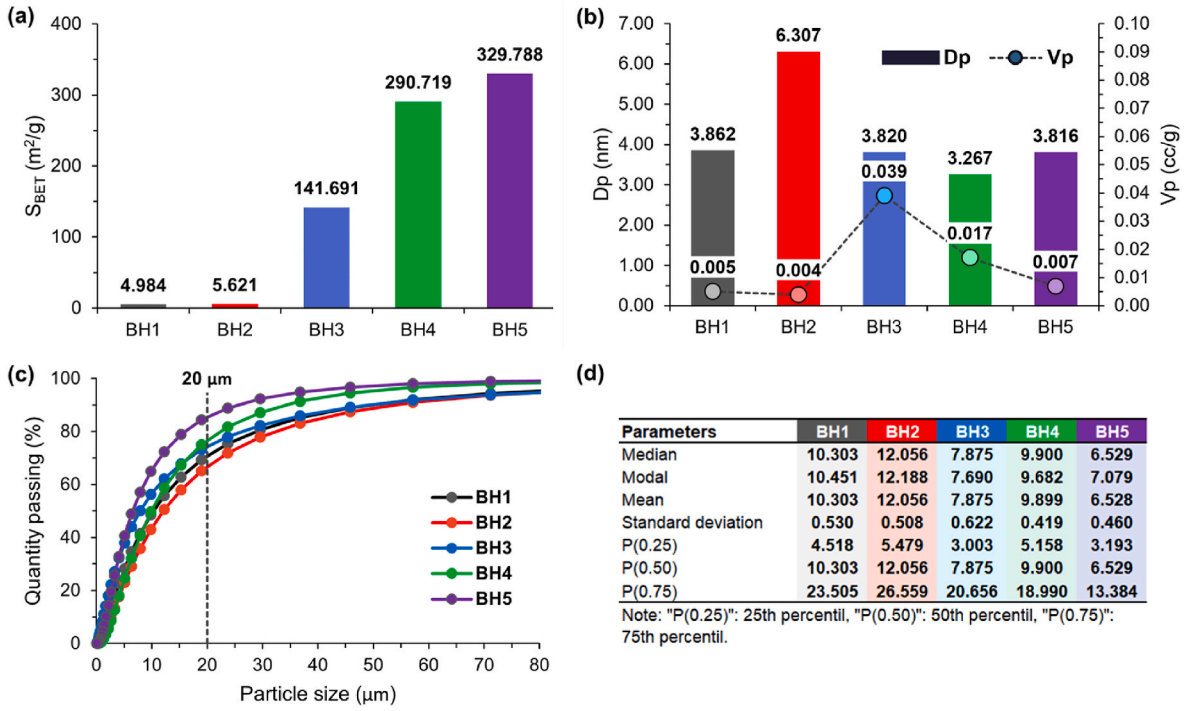

Parameters	BH1	BH2	BH3	BH4	BH5
Median	10.303	12.056	7.875	9.900	6.529
Modal	10.451	12.188	7.690	9.682	7.079
Mean	10.303	12.056	7.875	9.899	6.528
Standard deviation	0.530	0.508	0.622	0.419	0.460
P(0.25)	4.518	5.479	3.003	5.158	3.193
P(0.50)	10.303	12.056	7.875	9.900	6.529
P(0.75)	23.505	26.559	20.656	18.990	13.384

Note: "P(0.25)": 25th percentil, "P(0.50)": 50th percentil, "P(0.75)": 75th percentil.

Fig. 4. Physical properties of the biochar samples: (a) S_{BET}, (b) Dp versus Vp, (c) particle size distribution, and (d) descriptive parameters of particle size distribution.

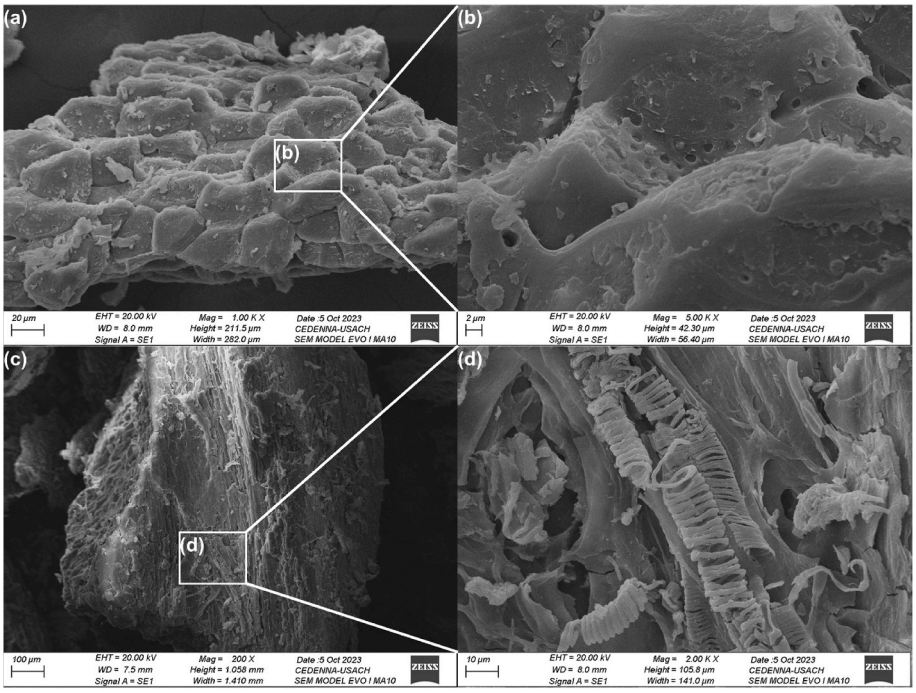

Fig. 5. SEM micrographs of HS at different magnifications: a) micrography at 1.00KX; b) zoom micrograph at 5.00KX; c) micrograph at 200X; and d) zoom micrograph at 2.00KX.

ZP –25 mV) [73]; sunflower seed husk (pH 9.07 and ZP –34.8 mV) [72]; rice chaff and wild sugar cane (both with pH 9 and ZP –7 and −10 mV) [69]; and purple sandspurry, fir and African palm (pH 9.58, 8.9 and 8.26 and ZP –48.7, −58.85 and −56.2 mV respectively) [71].

Fig. 8 shows the yield achieved in biochar production. According to the results, pyrolysis temperatures below 550 °C increased the content of solid subproducts in the form of biochar, while diminishing the liquid and gaseous fractions (i.e., bio-oil and syngas respectively). Pyrolysis at 300 °C produced greater biochar generation, between 19 and 24% higher than the quantities generated at 550 °C, depending on the residence time used (3 or 1 h respectively). In pyrolysis at 550 °C, biochar production was similar at both residence times. This may be explained by the fact that high temperatures cause rapid, complete decomposition of the lignocellulosic components of the HS, favouring the formation of the liquid and/or gaseous fractions [75,76]. On the other hand, the production yield of these biochar samples exceeded that of other

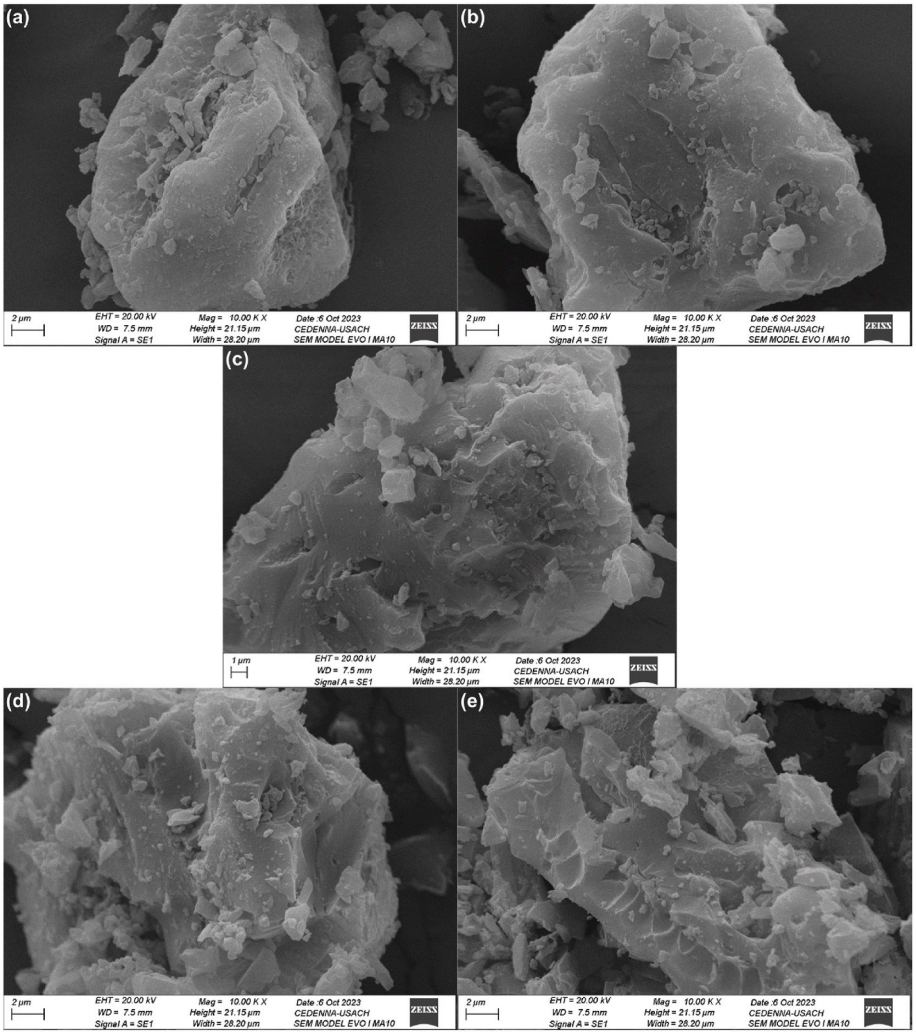

Fig. 6. SEM micrographs of the biochar samples: (a) BH1, (b) BH2, (c) BH3, (d) BH4 and (e) BH5.

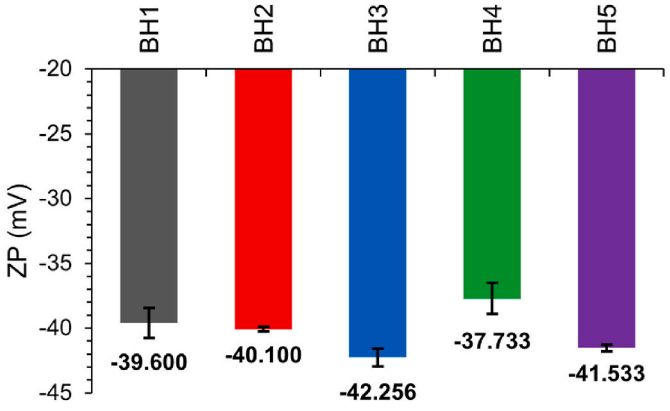

Fig. 7. Z-potential (ZP) of the biochars.

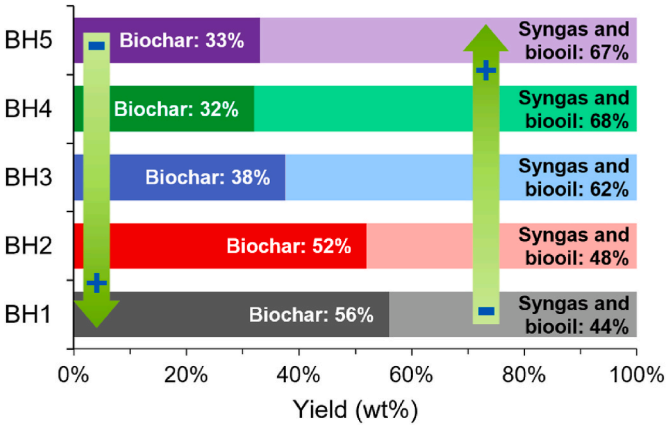

Fig. 8. Production yield of HS biochar by slow pyrolysis.

biomasses such as rice chaff or maize cobs, which yielded 26.8% and 23.2% biochar at 550 °C, respectively [77]. This may be because HS have a higher lignin content [48].

3.1.3. *Antioxidant properties*

Table 5 summarises the antioxidant properties of HS and other agro-industrial wastes registered as a reference. It can be observed that HS have an antioxidant activity lying between those of bean hulls and pistachio shells [78,79]. However, the recorded values depend on the analytical method used (i.e., ORAC, TEAC, DPPH, or CUPRAC) and the intrinsic properties of each shell. The latter is associated with the TPC, since in general a direct correlation is found between the antioxidant activity and the TPC [80]. In the case of HS, the TPC may be attributable to their phenolic compounds, such as phenolic acids, flavonoids, tannins, diarylheptanoids and lignins [7,10,14]. This underscores their role

Table 5
Antioxidant properties of European hazelnut shells and other agro-industrial waste products.

Sample	ORAC (μmol·100 g^{-1})	TEAC (μmol·g^{-1})	DPPH (μmol·g^{-1})	CUPRAC (μmol·g^{-1})	TPC (mg·100 g^{-1})
Bean hulls [78]	1964.000	–	–	–	–
European hazelnut shells, HS	11,137.800	10.030	9.290	22.850	270.610
Pistachio shell [79]	16,100.000	106.000	–	–	–

as a valuable source of natural antioxidant compounds, reinforcing the hypothesis that HS can be utilized as a biobased additive for asphalt binder. They may also prove beneficial as health-enhancing ingredients in functional foods, food supplements, and nutraceuticals [81].

After evaluation using the ORAC, TEAC, DPPH and CUPRAC methods (Fig. 9(a)–(d)), the factorial model indicated that the pyrolysis temperature, the residence time and the interaction between these factors generate a significant effect on the antioxidant activity of the biochar (P-values <0.05). Thus, as the pyrolysis temperature and residence time are increased, the antioxidant activity of the biochar compared to

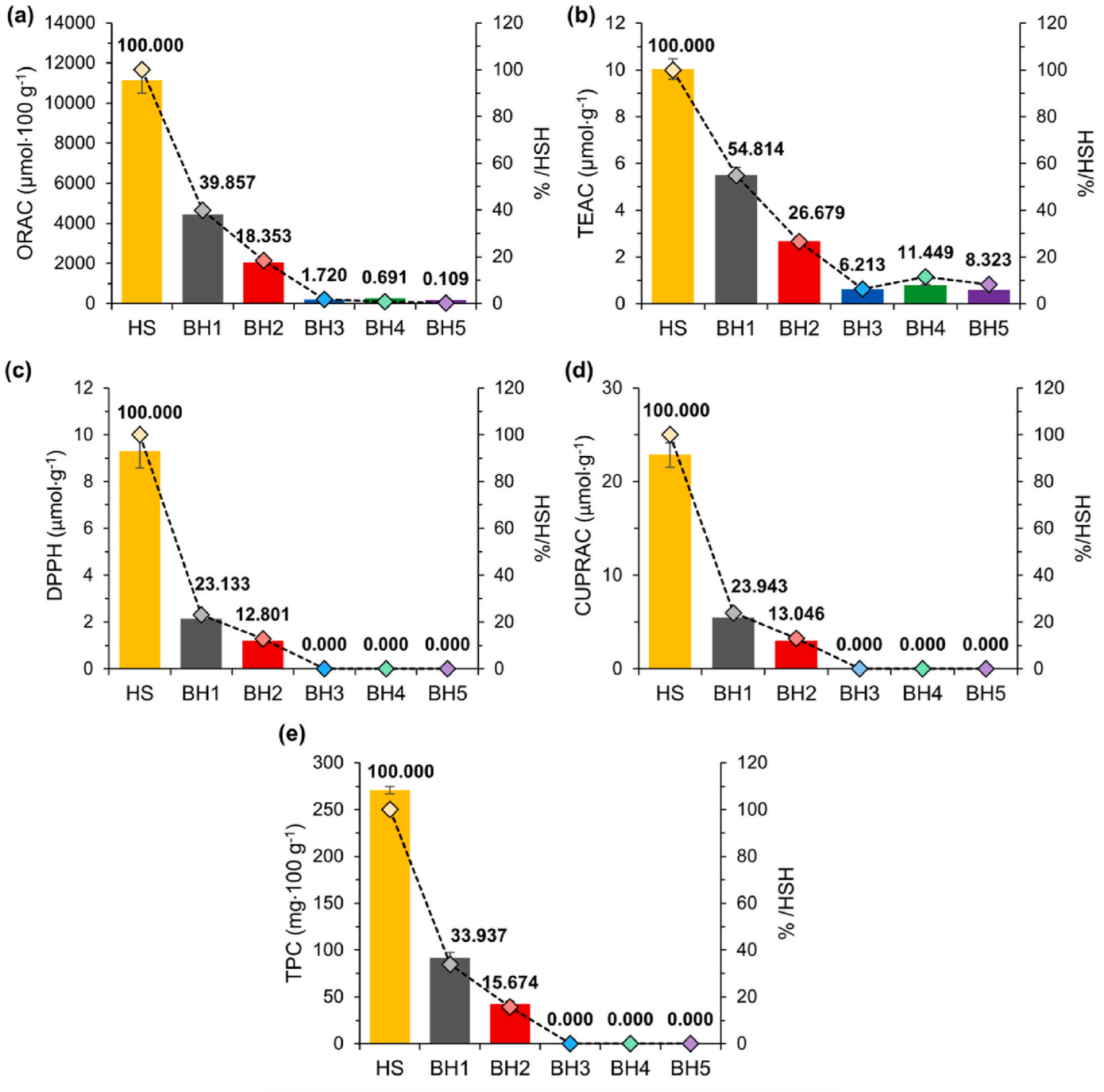

Fig. 9. Antioxidant properties of biochar together with the results for HS: antioxidant activity measured by the method (a) ORAC, (b) TEAC, (c) DPPH, (d) CUPRAC, and (e) total phenolic content (TPC) by Folin-Ciocalteu method.

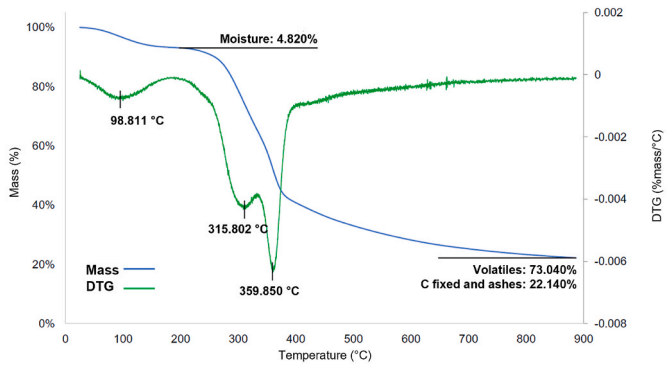

Fig. 10. Thermogravimetric analysis (TGA-DGT) of HS.

that of HS diminish significantly. In this case, the biochar pyrolyzed at 300 °C for 1 h (BH1) retained the highest antioxidant capacity, varying between 23 and 54% of that of HS, depending on the method used. In contrast, the biochar pyrolyzed at 550 °C for 3 h (BH5) produced the lowest values; the results were evaluated as trace levels by the DPPH and CUPRAC methods. When these results are compared with the TPC (Fig. 9 (e)), the behaviour coincides, showing a falling trend with increasing pyrolysis temperature and time. These conditions could therefore produce greater degradation of the antioxidant compounds in the HS [7,10,14,82]. Furthermore, biochar would tend to be generated with a diminished capacity to reduce or inhibit oxidation [80].

3.1.4. Thermal behaviour

Fig. 10 shows the thermal behaviour of HS up to 900 °C. A reduction of 77.86% in the total mass of the sample is observed (blue curve), attributed to physical and chemical reactions induced by temperature effect. First, the water adsorbed physically by the HS evaporates at temperatures between 25 and 100 °C. Subsequently, the organic material burns, followed by the elimination of chemical water [83]. The decomposition of the hemicellulose and the cellulose occurs between 120 and 350 °C, while the lignin decomposes at temperatures above 350 °C [47,60]. Greater mass loss occurs around these temperatures, leaving 22.14% (w) of ash. Otherwise, analysis of the differential thermogravimetry (DTG) curve (green curve) reveals three peaks: the first at 98.81 °C is attributed to the loss of moisture in the sample, the second at 315.80 °C corresponds to the degradation of hemicellulose, and the third at 359.85 °C is indicative of cellulose decomposition.

3.2. Characterisation of the asphalt binder modified with biochar

3.2.1. Physical interaction

Fig. 11 shows the distribution of the biochar in the asphalt, comparing a standard sample (Fig. 11(a)) with samples containing 5% w/w of biochar, see Fig. 11(b)–(f). The observations indicate that the biochar does not dissolve in the asphalt binder. Nevertheless, the dispersion of the particles can be considered optimal, with a homogeneous distribution inside the asphalt matrix. This result may be attributed to the modification process, and to the stability imparted by the ZP of the biochar [71]. In the study of Martínez-Toledo et al. [27] a similar distribution was observed for asphalt binder modified with oat hull biochar, indicating homogeneous integration between the two materials. This promotes improved rotational viscosity, penetration, and softening point, among other characteristics. The images obtained also confirm the results for particle size distribution observed in Fig. 4(c) and (d), showing that biochar pyrolyzed at 550 °C for 3 h presents the smallest particle size.

3.2.2. Chemical interaction between the asphalt binder and the biochar

Fig. 12(a) shows the IR spectra of the HS and the control asphalt binders (i.e., AB and AB+0). The asphalt binders are seen to be similar (superimposition of spectra) and are characterised by peaks attributable to functional groups of hydrocarbon, carbon and oxygen consistent with their nature [84]. The stretching observed include the following: CH_3 and $–CH_2$ in the 2918 and 2850 cm^{-1} bands respectively, corresponding to aliphatic compounds; –C═C around the 1586 and 1454 cm^{-1} bands, corresponding to alkenes; and finally, –C–O in the 1375 cm^{-1} band. Additionally, HS are characterised by the presence of functional groups related with lignocellulosic compounds (see Fig. 3). When the asphalt binder is mixed with each biochar, an increase is observed in the transmittance of the 1744 cm^{-1} band of the –C═O carbonyl group and the 1210 cm^{-1} band of the –COC– group after the modification procedure (see Fig. 12(b)). This occurred in the asphalt binders with biochar pyrolyzed at 300 °C for 1 h (AB + BH1) and 550 °C for 1 h (AB + BH4), indicating that these biochar samples are interacting chemically with

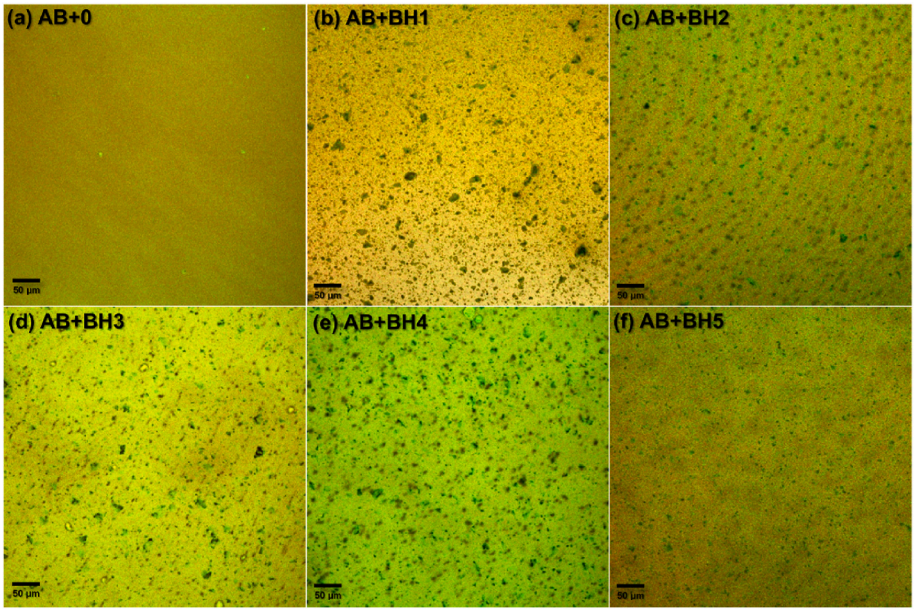

Fig. 11. Confocal laser microscopy photographs of the modified asphalt binders. The biochar particles are observed as black spots against the yellow ground of the asphalt binder.

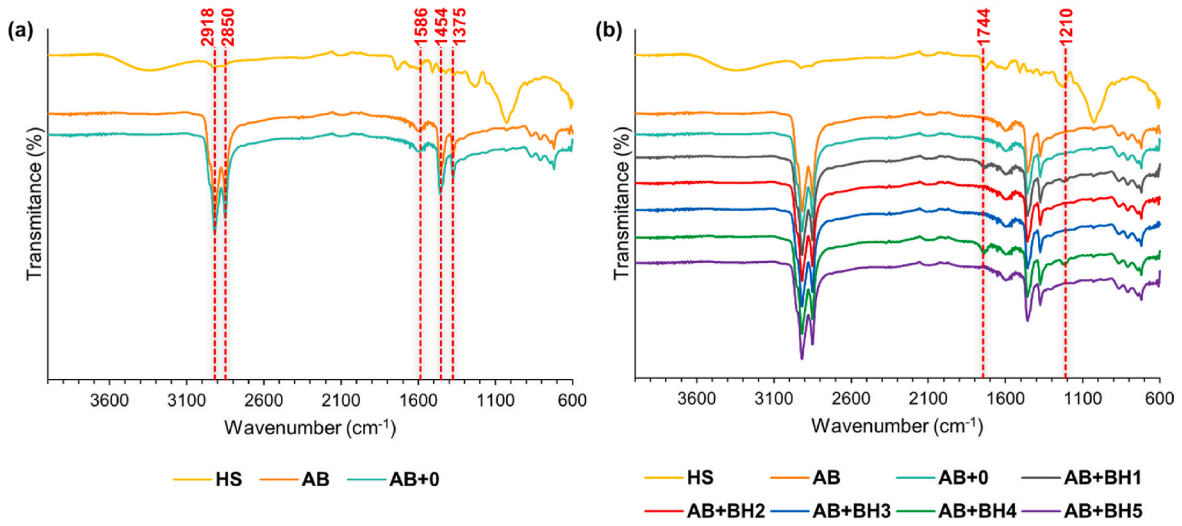

Fig. 12. IR spectra: (a) HS and the control asphalt binders AB and AB+0, and (b) functional groups of the interaction between asphalt binder and biochar.

the asphalt binder. According to the literature, the –C═O carbonyl group could improve the rheological properties of the asphalt binder such as resistance to fatigue and rutting [58], while the –COC– groups and phenols associated with lignin may improve resistance to ageing and rutting [54,85].

To explore the FT-IR findings further, XPS analysis was used to identify and quantify functional groups in AB, AB + BH1 and AB + BH4, using a scan from 0 to 1350 eV (Fig. 13(a), (b) and (c) respectively) and high resolution scans in the C 1s and O 1s bands (Fig. 13(d)–(i)). The samples are observed to present the same contributions in C 1s, but with different intensities (Fig. 13(d)–(f)). AB + BH1 presented the highest concentration of COH, CO and Cs2 located close to 286 eV, with an increase of 1.54% over AB. In the case of AB + BH4, the C–C and C═C located at 284 eV reached the highest concentration with 85.31%, i.e. 3% higher than in AB. The area attributable to COO, COOH and C═O located close to 288 eV tends to diminish by between 1.96 and 3.74% in the modified asphalt binders. It is therefore assumed that the area quantified by XPS corresponds principally to the C═O carbonyl group due to the peak observed in the IR spectra of Fig. 12(b) and (c). In O 1s, the AB + BH1 sample also showed an increase in functional groups over AB; COH and COC (533 eV) increased by 2.78%, and C═O and sulphate (532 eV) by 10.34% (Fig. 13(g)–(i)). This agrees with the FT-IR results (see Fig. 12(a) and (b)). The CO and sulphite concentrations diminished by more than 11%. The COH and COC contents of AB + BH4 remained similar to those of AB; however, at 532 eV the area diminished, leaving only 28.49% attributable to C═O. A diminution was also observed in the contributions of CO and sulphite at 531 eV, but they were greater than those found in AB + BH1. Based on the findings, the variation in the amount of functional groups confirms a chemical interaction between the asphalt binder and the biochar. In the case of the biochar samples pyrolyzed at 300 °C for 1 h, the reactions tend to occur through C, O and H. In contrast, in the biochar pyrolyzed at 550 °C for 1 h, they occur principally through C due to their high carbon content (approx. 84%), and through the diminution of functional groups containing O and H, as a product of the pyrolysis temperature and time (see Table 3) [18,43,44].

4. Conclusions

This study assessed the impact of operational conditions during slow pyrolysis on the physicochemical and antioxidant properties of European hazelnut shell biochar, with the aim of exploring its potential as an asphalt binder modifier. Based on the obtained results, the following conclusions were drawn.

- The operational conditions of slow pyrolysis affect the physical-chemical properties of biochar. Higher pyrolysis temperatures and longer residence times increase the carbon content while decreasing oxygen and hydrogen, altering the functional groups on the biochar surface. Some groups disappear or transform. Additionally, higher temperatures create rougher, more porous surfaces, especially in biochar pyrolyzed at 550 °C for 1–3 h, due to enhanced degradation of lignocellulosic compounds. This results in heterogeneous, porous particles with a larger surface area, primarily forming mesopores. These changes improve the biochar's interaction with the asphalt binder and its distribution in the matrix.
- The antioxidant properties of European hazelnut shell were found to be high, retaining up to 40% at 300 °C for 1 h. However, this activity decreases with higher temperatures and longer residence times, nearly vanishing in biochar pyrolyzed at 425 °C and 550 °C. This reduction is linked to a decrease in phenolic compounds, with lower concentrations of total polyphenols correlating with the decline in antioxidant activity.
- Confocal laser microscopy reveals a good distribution of biochar in asphalt binder. FT-IR and XPS analyses confirm a chemical interaction between the binder and biochar, shown by changes in functional groups. At 300 °C for 1 h, reactions mainly involve C, O, and H, while at 550 °C for 1 h, carbon predominates, indicating these biochar samples may be effective modifiers.

Future research will focus on assessing the effect of biochar produced at varying pyrolysis temperatures on the physical, rheological, and ageing properties of asphalt binder. Key variables in biochar modification, including different biochar percentages and particle sizes, will be considered to determine the optimal biochar characteristics that enhance the properties of the modified asphalt binder. Following the selection of the most suitable biochar, the critical performance properties of asphalt mixtures incorporating the biochar-modified asphalt binder will be evaluated.

CRediT authorship contribution statement

Camila Martínez-Toledo: Writing – original draft, Validation, Methodology, Investigation, Formal analysis, Data curation. **Gonzalo Valdes-Vidal:** Writing – review & editing, Visualization, Validation, Supervision, Resources, Project administration, Methodology, Investigation, Funding acquisition, Formal analysis, Conceptualization. **Alejandra Calabi-Floody:** Validation, Supervision, Methodology, Investigation, Formal analysis. **María Eugenia González:** Validation,

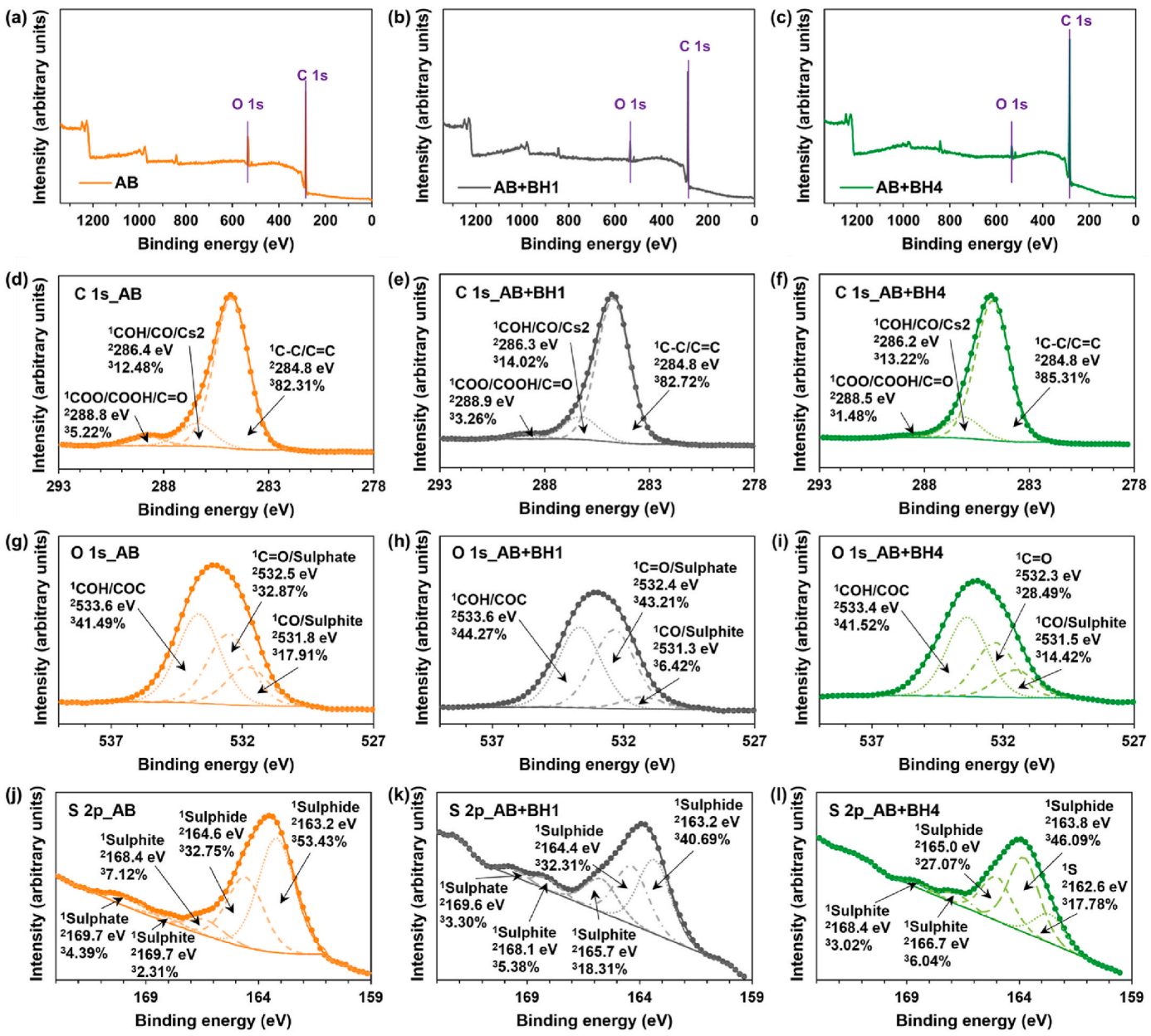

Fig. 13. XPS results for: (a), (b) and (c) survey of AB, AB + BH1 and AB + BH4; (d), (e) and (f) C 1s scan of AB, AB + BH1 and AB + BH4; (g), (h) and (i) O 1s scan of AB, AB + BH1 and AB + BH4. 1: Name; 2: location; and 3: concentration.

Methodology, Investigation, Formal analysis, Conceptualization. **Antonieta Ruiz:** Methodology, Formal analysis, Data curation. **Cristian Mignolet-Garrido:** Methodology, Investigation, Data curation. **Jose Norambuena-Contreras:** Writing – review & editing, Visualization, Validation, Supervision, Methodology, Investigation, Formal analysis, Conceptualization.

Funding

This research was funded by the National Research and Development Agency (ANID) of the Chilean Government, through ANID/FONDECYT Regular Research Project 2023 No 1230035.

Declaration of competing interest

The authors declare the following financial interests/personal relationships which may be considered as potential competing interests: Gonzalo Valdes Vidal reports financial support was provided by National Agency for Research and Development. If there are other authors, they declare that they have no known competing financial interests or personal relationships that could have appeared to influence the work reported in this paper.

Acknowledgements

The first author wishes to thank the National Research and Development Agency (ANID) of the Chilean Government for the financial support provided through his PhD scholarship grant N°. 21230892. The authors would like to thank Marcelo Tiznado Rivas for his support during the experimental programme of this work.

Data availability

Data will be made available on request.

References

[1] H. Zhang, C. Zhu, J. Yu, C. Shi, D. Zhang, Influence of surface modification on physical and ultraviolet aging resistance of bitumen containing inorganic nanoparticles, Constr. Build. Mater. 98 (Nov. 2015) 735–740, https://doi.org/10.1016/j.conbuildmat.2015.08.138.

[2] Q. Yang, J. Lin, X. Wang, D. Wang, N. Xie, X. Shi, A review of polymer-modified asphalt binder: modification mechanisms and mechanical properties, Cleaner Mater. 12 (Jun) (2024), https://doi.org/10.1016/j.clema.2024.100255.

[3] EAPA, Learn about asphalt [Online]. Available: https://eapa.org/asphalt/. (Accessed 4 December 2024).

[4] M. Buncher, What Percentage of Our Roads Are Asphalt (Versus Concrete)? A Systematic and Objective Way to Measure, 34, 2019, pp. 7–12.

[5] Dirección de Vialidad, Red Vial Nacional Dimensionamiento Y Características 2023, Ministerio de Obras Públicas, 2023.

[6] M. Chen, J. Geng, C. Xia, L. He, Z. Liu, A Review of Phase Structure of SBS Modified Asphalt: Affecting Factors, Analytical Methods, Phase Models and Improvements, Elsevier Ltd., Aug. 02, 2021, https://doi.org/10.1016/j.conbuildmat.2021.123610.

[7] J. Zhao, X. Wang, H. Lin, Z. Lin, Hazelnut and its by-products: a comprehensive review of nutrition, phytochemical profile, extraction, bioactivities and applications, Food Chem. 413 (January) (2023) 135576, https://doi.org/10.1016/j.foodchem.2023.135576.

[8] FAO, "Agricultural statistical database," Food and Agriculture Organization of the United Nations. Accessed: January. 3, 2024. [Online]. Available: http://www.https//www.fao.org/faostat/es/#data/QCL/visualize.

[9] R. Herrera, J. Hemming, A. Smeds, O. Gordobil, S. Willför, J. Labidi, Recovery of bioactive compounds from hazelnuts and walnuts shells: quantitative–qualitative analysis and chromatographic purification, Biomolecules 10 (10) (2020) 1–16, https://doi.org/10.3390/biom10101363.

[10] A. Allegrini, P. Salvaneschi, B. Schirone, K. Cianfaglione, A. Di Michele, Multipurpose plant species and circular economy: Corylus avellana L. as a study case, Frontiers in Bioscience - Landmark 27 (1) (2022) 1–20, https://doi.org/10.31083/j.fbl2701011.

[11] K. Lewicka, Activated carbons prepared from hazelnut shells, walnut shells and peanut shells for high CO2 adsorption, Pol. J. Chem. Technol. 19 (2) (Jun. 2017) 38–43, https://doi.org/10.1515/pjct-2017-0025.

[12] E.Z. Hoşgün, D. Berikten, M. Kıvanç, B. Bozan, Ethanol production from hazelnut shells through enzymatic saccharification and fermentation by low-temperature alkali pretreatment, Fuel 196 (2017) 280–287, https://doi.org/10.1016/j.fuel.2017.01.114.

[13] B. Yuan, M. Lu, K.M. Eskridge, L.D. Isom, M.A. Hanna, Extraction, identification, and quantification of antioxidant phenolics from hazelnut (Corylus avellana L.) shells, Food Chem. 244 (Apr. 2018) 7–15, https://doi.org/10.1016/j.foodchem.2017.09.116.

[14] A. Di Michele, et al., Hazelnut shells as source of active ingredients: extracts preparation and characterization, Molecules 26 (21) (2021), https://doi.org/10.3390/molecules26216607.

[15] E.Z. Hoşgün, B. Bozan, Effect of different types of thermochemical pretreatment on the enzymatic hydrolysis and the composition of hazelnut shells, Waste Biomass Valorization 11 (7) (2020) 3739–3748, https://doi.org/10.1007/s12649-019-00711-z.

[16] A. Safavi, C. Richter, R. Unnthorsson, Mathematical modeling and experiments on pyrolysis of walnut shells using a fixed-bed reactor, ChemEngineering 6 (6) (2022), https://doi.org/10.3390/chemengineering6060093.

[17] P.R. Yaashikaa, P.S. Kumar, S. Varjani, A. Saravanan, A critical review on the biochar production techniques, characterization, stability and applications for circular bioeconomy, Biotechnology Reports 28 (2020) e00570, https://doi.org/10.1016/j.btre.2020.e00570.

[18] A. Tomczyk, Z. Sokołowska, P. Boguta, Biochar physicochemical properties: pyrolysis temperature and feedstock kind effects, Rev. Environ. Sci. Biotechnol. 19 (1) (2020) 191–215, https://doi.org/10.1007/s11157-020-09523-3.

[19] B. Babinszki, et al., Effect of slow pyrolysis conditions on biocarbon yield and properties: characterization of the volatiles, Bioresour. Technol. 338 (2021), https://doi.org/10.1016/j.biortech.2021.125567.

[20] B. Handiso, T. Pääkkönen, B.P. Wilson, Effect of pyrolysis temperature on the physical and chemical characteristics of pine wood biochar, Waste Manag. Bulletin 2 (4) (Dec. 2024) 281–287, https://doi.org/10.1016/j.wmb.2024.11.008.

[21] R. Potnuri, D.V. Surya, C.S. Rao, A. Yadav, V. Sridevi, N. Remya, A review on analysis of biochar produced from microwave-assisted pyrolysis of agricultural waste biomass, J. Anal. Appl. Pyrolysis 173 (Aug) (2023), https://doi.org/10.1016/j.jaap.2023.106094.

[22] N. Abdullah, R. Mohd Taib, N.S. Mohamad Aziz, M.R. Omar, N. Md Disa, Banana pseudo-stem biochar derived from slow and fast pyrolysis process, Heliyon 9 (1) (Jan. 2023) e12940, https://doi.org/10.1016/j.heliyon.2023.e12940.

[23] J. Lehmann, S. Joseph, Biochar for Environmental Management: Science, Technology and Implementation, second ed., Taylor & Francis, 2015 [Online]. Available: https://books.google.es/books?id=gWDABgAAQBAJ.

[24] G. Enaime, A. Baçaoui, A. Yaacoubi, M. Lübken, Biochar for Wastewater Treatment-Conversion Technologies and Applications, MDPI AG, May 01, 2020, https://doi.org/10.3390/app10103492.

[25] European asphalt pavement association and national asphalt pavement association, The Asphalt Paving Industry A Global Perspective - 2nd edition (2011) [Online]. Available: http://www.asphaltpavement.org/images/stories/GL_101_Edition_3.pdf.

[26] United Nations, The sustainable development goals report 2024 [Online]. Available: https://unstats.un.org/sdgs/report/2024/, 2024. (Accessed 31 December 2024).

[27] C. Martínez-Toledo, G. Valdés-Vidal, A. Calabi-Floody, M.E. González, O. Reyes-Ortiz, Effect of biochar from oat hulls on the physical properties of asphalt binder, Materials 15 (19) (2022), https://doi.org/10.3390/ma15197000.

[28] X. Zhou, et al., Effects of biochar on the chemical changes and phase separation of bio-asphalt under different aging conditions, J. Clean. Prod. 263 (2020) 121532, https://doi.org/10.1016/j.jclepro.2020.121532.

[29] R. Zhang, Q. Dai, Z. You, H. Wang, C. Peng, Rheological performance of bio-char modified asphalt with different particle sizes, Appl. Sci. 8 (9) (2018) 1–15, https://doi.org/10.3390/app8091665.

[30] X. Gan, W. Zhang, Application of biochar from crop straw in asphalt modification, PLoS One 16 (2 February) (2021) 1–11, https://doi.org/10.1371/journal.pone.0247390.

[31] F. Ma, et al., Biochar for asphalt modification: a case of high-temperature properties improvement, Sci. Total Environ. 804 (2022) 150194, https://doi.org/10.1016/j.scitotenv.2021.150194.

[32] C. Hu, J. Feng, N. Zhou, J. Zhu, S. Zhang, Hydrochar from corn stalk used as bio-asphalt modifier: high-temperature performance improvement, Environ. Res. 193 (July 2020) (2021) 110157, https://doi.org/10.1016/j.envres.2020.110157.

[33] R.C. Walters, E.H. Fini, Taher Abu-Lebdeh, Enhancing asphalt rheological behavior and aging susceptibility using bio-char and nano-clay, Am. J. Eng. Appl. Sci. 7 (1) (2014) 66–76, https://doi.org/10.3844/ajeassp.2014.66.76.

[34] K.H. Tan, Soil Sampling, Preparation, and Analysis, second ed., CRC Press, 2005 https://doi.org/10.1201/9781482274769.

[35] G. Cao, E. Sofic, R. Prior, Antioxidant and prooxidant behavior of flavonoids: structure-activity relationships, Free Radic. Biol. Med. 22 (5) (1997) 749–760.

[36] E. Pastrana-Bonilla, C.C. Akoh, S. Sellappan, G. Krewer, Phenolic content and antioxidant capacity of muscadine grapes, J. Agric. Food Chem. 51 (18) (Aug. 2003) 5497–5503, https://doi.org/10.1021/jf030113c.

[37] J. Parada, et al., Effect of fertilization and arbuscular mycorrhizal fungal inoculation on antioxidant profiles and activities in Fragaria ananassa fruit, J. Sci. Food Agric. 99 (3) (2019) 1397–1404, https://doi.org/10.1002/jsfa.9316.

[38] P.D. Maldonado, I. Rivero-Cruz, R. Mata, J. Pedraza-Chaverrí, Antioxidant activity of A-type proanthocyanidins from Geranium niveum (Geraniacea), J. Agric. Food Chem. 53 (6) (Mar. 2005) 1996–2001, https://doi.org/10.1021/jf0483725.

[39] J. Ribeiro, L. Magalhães, S. Reis, J. Lima, M. Segundo, High-throughput total cupric ion reducing antioxidant capacity of biological samples determined using flow injection analysis and microplate-based methods, Anal. Sci. (2011) 483–488.

[40] V. Singleton, R. Orthofer, R. Lamuela-Raventos, Analysis of total phenols and other oxidation substrates and antioxidants by means of Folin-Ciocalteu reagent, in: first ed.Methods in Enzymology, 299, Elsevier S&T, Cambridge, MA, USA, 1999, pp. 152–178.

[41] M. Ellena, A. Montenegro, P. Sandoval, A. González, G. Azócar, Avellano europeo: Establecimiento y formación de la estructura productiva, in: Temuco, Chile: Boletín INIA - Instituto de Investigaciones Agropecuarias, 274th ed., 2013 [Online]. Available: https://hdl.handle.net/20.500.14001/7684. (Accessed 13 September 2023).

[42] M. Ellena, A. Montenegro, A. González, P. Sandoval, Fertilización en Avellano Europeo, ch. 5, in: ón Carillanca (2018) El avellano europeo en Chile. Una década de recopilación e investigación, 36th ed., Temuco, Chile: Colección Libros INIA - Instituto de Investigaciones Agropecuarias, 2018, pp. 114–152 [Online]. Available: https://hdl.handle.net/20.500.14001/3591. (Accessed 13 September 2023).

[43] J. Lehmann, M.C. Rillig, J. Thies, C.A. Masiello, W.C. Hockaday, D. Crowley, Biochar effects on soil biota - a review, Soil Biol. Biochem. 43 (9) (2011) 1812–1836, https://doi.org/10.1016/j.soilbio.2011.04.022.

[44] M.E. González, et al., Effects of pyrolysis conditions on physicochemical properties of oat hull derived biochar, Bioresources 12 (1) (2017) 2040–2057, https://doi.org/10.15376/biores.12.1.2040-2057.

[45] N.M. Noor, A. Shariff, N. Abdullah, N. Syairah, M. Aziz, Temperature effect on biochar properties from slow pyrolysis of coconut flesh waste, 2019.

[46] O. Mašek, P. Brownsort, A. Cross, S. Sohi, Influence of production conditions on the yield and environmental stability of biochar, Fuel (Jan. 2013) 151–155, https://doi.org/10.1016/j.fuel.2011.08.044.

[47] N. Kaya, Z. Yıldız, S. Ceylan, Preparation and characterisation of biochar from hazelnut shell and its adsorption properties for methylene blue dye, J. Polytech. (Jan. 2018), https://doi.org/10.2339/politeknik.386963.

[48] C. Zhao, X. Liu, A. Chen, J. Chen, W. Lv, X. Liu, Characteristics evaluation of biochar produced by pyrolysis from waste hazelnut shell at various temperatures, Energy Sources, Part A Recovery, Util. Environ. Eff. (2020), https://doi.org/10.1080/15567036.2020.1754530.

[49] M. Stjepanović, N. Velić, M. Habuda-Stanić, Modified hazelnut shells as a novel adsorbent for the removal of nitrate from wastewater, Water (Switzerland) 14 (5) (Mar. 2022), https://doi.org/10.3390/w14050816.

[50] E. Altintig, B. Sarıcı, S. Karataş, Prepared activated carbon from hazelnut shell where coated nanocomposite with Ag+ used for antibacterial and adsorption properties, Environ. Sci. Pollut. Control Ser. 30 (5) (Jan. 2023) 13671–13687, https://doi.org/10.1007/s11356-022-23004-w.

[51] D. Licursi, et al., In-depth characterization of valuable char obtained from hydrothermal conversion of hazelnut shells to levulinic acid, Bioresour. Technol. 244 (Nov. 2017) 880–888, https://doi.org/10.1016/j.biortech.2017.08.012.

[52] İ.M. Hasdemir, E. Yılmazoğlu, S. Güngör, B. Hasdemir, Adsorption of acetic acid onto activated carbons produced from hazelnut shell, orange peel, and melon seeds, Appl. Water Sci. 12 (12) (Dec. 2022), https://doi.org/10.1007/s13201-022-01797-y.

[53] H. Düdder, A. Wütscher, R. Stoll, M. Muhler, Synthesis and characterization of lignite-like fuels obtained by hydrothermal carbonization of cellulose, Fuel 171 (May 2016) 54–58, https://doi.org/10.1016/j.fuel.2015.12.031.
[54] A. Kumar, R. Choudhary, R. Narzari, R. Kataki, S.K. Shukla, Evaluation of bio-asphalt binders modified with biochar: a pyrolysis by-product of Mesua ferrea seed cover waste, Cogent Eng 5 (1) (2018) 1–15, https://doi.org/10.1080/23311916.2018.1548534.
[55] T. Pan, A first-principles based chemophysical environment for studying lignins as an asphalt antioxidant, Constr. Build. Mater. 36 (Nov. 2012) 654–664, https://doi.org/10.1016/j.conbuildmat.2012.06.012.
[56] R.C. Williams, N.S. McCready, The Utilization of Agriculturally Derived Lignin as an Antioxidant in Asphalt Binder, 14, InTrans Project Reports, 2008 [Online]. Available: http://lib.dr.iastate.edu/intrans_reports/14. (Accessed 28 March 2023).
[57] F. Pahlavan, A. Lamanna, K.B. Park, S.F. Kabir, J.S. Kim, E.H. Fini, Phenol-rich bio-oils as free-radical scavengers to hinder oxidative aging in asphalt binder, Resour. Conserv. Recycl. 187 (Dec) (2022), https://doi.org/10.1016/j.resconrec.2022.106601.
[58] H. Yao, Q. Dai, Z. You, Fourier Transform Infrared Spectroscopy characterization of aging-related properties of original and nano-modified asphalt binders, Constr. Build. Mater. 101 (Dec. 2015) 1078–1087, https://doi.org/10.1016/j.conbuildmat.2015.10.085.
[59] M.E. González, et al., Biochar derived from agricultural and forestry residual biomass: characterization and potential application for enzymes immobilization, J. Biobased Mater. Bioenergy 7 (6) (Dec. 2013) 724–732, https://doi.org/10.1166/jbmb.2013.1373.
[60] S.H. Ghaffar, M. Fan, Structural analysis for lignin characteristics in biomass straw (Oct. 2013), https://doi.org/10.1016/j.biombioe.2013.07.015.
[61] M. Keiluweit, P.S. Nico, M. Johnson, M. Kleber, Dynamic molecular structure of plant biomass-derived black carbon (biochar), Environ. Sci. Technol. 44 (4) (2010) 1247–1253, https://doi.org/10.1021/es9031419.
[62] H. Kawamoto, M. Murayama, S. Saka, Pyrolysis behavior of levoglucosan as an intermediate in cellulose pyrolysis: polymerization into polysaccharide as a key reaction to carbonized product formation, J. Wood Sci. 49 (5) (2003) 469–473, https://doi.org/10.1007/s10086-002-0487-5.
[63] Y. Sik Ok, S.M. Uchimiya, S.X. Chang, Nanthi Bolan, Biochar: Production, Characterization, and Applications, CRC Press, 2015.
[64] S. Zhao, B. Huang, X.P. Ye, X. Shu, X. Jia, Utilizing bio-char as a bio-modifier for asphalt cement: a sustainable application of bio-fuel by-product, Fuel 133 (Oct. 2014) 52–62, https://doi.org/10.1016/j.fuel.2014.05.002.
[65] F. Rouquerol, et al., "Adsorption by powders and porous solids principles, methodology and applications second edition," [Online]. Available: http://elsevier.com/locate/permissions, 2014.
[66] H. Haykiri-Acma, S. Yaman, S. Kucukbayrak, Comparison of the thermal reactivities of isolated lignin and holocellulose during pyrolysis, Fuel Process. Technol. 91 (7) (Jul. 2010) 759–764, https://doi.org/10.1016/j.fuproc.2010.02.009.
[67] S.P.J.M. Carrott, M.M.L. Ribeiro Carrott, Lignin - from natural adsorbent to activated carbon: A review (Sep. 2007), https://doi.org/10.1016/j.biortech.2006.08.008.
[68] R. Zhang, Q. Dai, Z. You, H. Wang, C. Peng, Rheological performance of bio-char modified asphalt with different particle sizes, Appl. Sci. 8 (9) (Sep. 2018), https://doi.org/10.3390/app8091665.
[69] Y. Barría, A. Burbano, A. James, G. Gascó, A. Méndez, Sorption capacity of biochars obtained by gasification of rice husks and wild sugarcane: removal of malachite green and arsenic from water solutions, Biomass Convers Biorefin (2023), https://doi.org/10.1007/s13399-023-04325-3.
[70] R.J. Hunter, Zeta Potential in Colloid Science: Principles and Applications, Academic Press, 1981.
[71] K. Barrientos, et al., Synthesis, characterization and ecotoxicity evaluation of biochar-derived carbon dots from spruce tree, purple moor-grass and african oil palm, Processes 9 (7) (Jul. 2021), https://doi.org/10.3390/pr9071095.
[72] A.A. Burbano, G. Gascó, F. Horst, V. Lassalle, A. Méndez, Production, characteristics and use of magnetic biochar nanocomposites as sorbents, Biomass Bioenergy 172 (May 2023), https://doi.org/10.1016/j.biombioe.2023.106772.
[73] S. Mehmood, et al., Chitosan modified biochar increases soybean (Glycine max l.) resistance to salt-stress by augmenting root morphology, antioxidant defense mechanisms and the expression of stress-responsive genes, Plants 9 (9) (Sep. 2020) 1–25, https://doi.org/10.3390/plants9091173.
[74] Asphalt Institute, Moisture Sensitivity MS-24, First, 2007.
[75] A. Selvarajoo, D. Oochit, Effect of pyrolysis temperature on product yields of palm fibre and its biochar characteristics, Mater Sci Energy Technol 3 (Jan. 2020) 575–583, https://doi.org/10.1016/j.mset.2020.06.003.
[76] A. Fuso, et al., Potential Valorization of Hazelnut Shells through Extraction, Purification and Structural Characterization of Prebiotic Compounds: A Critical Review, MDPI AG, Jun. 01, 2021, https://doi.org/10.3390/foods10061197.
[77] P.T. Williams, N. Nugranad, Comparison of products from the pyrolysis and catalytic pyrolysis of rice husks [Online]. Available: www.elsevier.com/locate/energy, 2000.
[78] B.D. Oomah, A. Corbé, P. Balasubramanian, Antioxidant and anti-Inflammatory activities of bean (Phaseolus vulgaris L.) Hulls, J. Agric. Food Chem. 58 (14) (Jul. 2010) 8225–8230, https://doi.org/10.1021/jf1011193.
[79] N. Cardullo, M. Leanza, V. Muccilli, C. Tringali, Valorization of agri-food waste from pistachio hard shells: extraction of polyphenols as natural antioxidants, Resources 10 (5) (May 2021), https://doi.org/10.3390/resources10050045.
[80] M.S. Fernández-Pachón, D. Villaño, A.M. Troncoso, M.C. García-Parrilla, Revisión de los métodos de evaluación de la actividad antioxidante in vitro del vino y valoración de sus efectos in vivo, Arch. Latinoam. Nutr. 56 (Feb. 2006) 110–122 [Online]. Available: http://ve.scielo.org/scielo.php?script=sci_arttext&pid=S0004-06222006000200002&nrm=iso.
[81] T. Esposito, et al., Hazelnut (Corylus avellana l.) shells extract: phenolic composition, antioxidant effect and cytotoxic activity on human cancer cell lines, Int. J. Mol. Sci. 18 (2) (Feb. 2017), https://doi.org/10.3390/ijms18020392.
[82] I. Volf, I. Ignat, M. Neamtu, V.I. Popa, Thermal stability, antioxidant activity, and photo-oxidation of natural polyphenols, Chem. Pap. 68 (1) (Jan. 2014) 121–129, https://doi.org/10.2478/s11696-013-0417-6.
[83] A. Yavaş, E. Atan, M. Sutcu, Self-cleaning and photocatalytic properties of eco-friendly clay-based facing bricks from industrial and natural wastes, Environ. Sci. Pollut. Control Ser. (Jul. 2023), https://doi.org/10.1007/s11356-023-27798-1.
[84] R.N. Hunter, The Shell Bitumen Handbook, sixth ed., Shell Bitumen UK, 2014.
[85] R. Ghabchi, Effect of lignin type as an additive on rheology and adhesion properties of asphalt binder, Solids 3 (4) (Dec. 2022) 603–619, https://doi.org/10.3390/solids3040038.